

# Raman spectroscopic Investigations of dynamics of polar nano regions in Pr-doped SrTiO<sub>3</sub>

Vivek Dwij, Binoy Krishna De, Shekhar Tyagi, Gaurav Sharma and V.G. Sathe\*

UGC-DAE Consortium for Scientific Research,

D. A. University Campus, Khandwa Road, Indore-452001, INDIA

\*Corresponding author e-mail: vasant@csr.res.in

## Abstract

The dynamics of Polar nano regions in a relaxor ferroelectric is studied using temperature dependent Raman spectroscopy. In Pr doped SrTiO<sub>3</sub> system, TO<sub>2</sub> polar mode frequency renormalizes due to local ferroelectric order resulting in anomalous softening below a temperature that matches with the dielectric maxima temperature in all the compositions. The weak local polar distortions were found to be present in all the doped compositions up to temperatures that are substantially higher compared to Burns temperature. The intensity of the TO<sub>2</sub> phonon mode showed modulation across the freezing temperature of the PNR dynamics and the dielectric maxima temperature. It is shown that the antiferrodistortive instability cooperates and supports the polar instability in this relaxor system.

## Introduction:

Relaxor ferroelectrics are important technological materials and hence been investigated actively for long time due to their superiority over normal ferroelectrics [1,2,3,4]. The difference between the ferroelectrics and relaxor ferroelectrics comes from the correlation length of the off-centred ions. Another noticeable property of relaxors is huge but diffuse dielectric maxima it displays when measured as a function of temperature ( $T_m$ ) and dispersion in  $T_m$  when measured as a function of frequency. These properties are generally attributed to the growth and dynamics of the polar nano regions (PNRs) in the matrix of a paraelectric phase. The nucleation of PNRs is marked by a temperature known as Burns temperature  $T_B$ . Below  $T_B$  several characteristic temperatures marking the properties of PNRs are defined in literature that are summarised by Mihailova et al [5] as follows: (i) a fully dynamic stage above  $T_B$ , (ii) quasidynamic behavior between  $T_B$  and  $T^*$ ;  $T^*$  is defined as the temperature below  $T_B$  where initial freezing of the polar nano regions start, (iii) quasistatic between  $T^*$  and  $T_f$ ;  $T_f$  is defined as the freezing temperature observed just below  $T_m$  where the system undergoes from ergodic to non-ergodic state with static coupled PNRs and (iv) static below  $T_f$ . Thus in a relaxor ferroelectrics the length scale and dynamics of PNRs play a major role in shaping the physical response of the system.

The Polar Regions are produced by off-centering of A-site and/or B-site ions in the perovskite systems. For example in lead based relaxors the Pb ions is known to be displaced from its high symmetry position along with displacement of B-site cations which is Nb in case of Pb(Zr)NbO<sub>3</sub> [6,7,8,9,10]. Similarly, lead free relaxor systems like Na<sub>0.5</sub>Bi<sub>0.5</sub>TiO<sub>3</sub> and KTa<sub>1-x</sub>Nb<sub>x</sub>O<sub>3</sub> also show A-site displacements producing non-centrosymmetry in the system [11,12]. The local off-

centred regions and induced relaxor behaviour comes from the local strain fields generated due to compositional fluctuation of the doped ions. For example, un-doped Pb(Zr)TiO<sub>3</sub>, BaTiO<sub>3</sub> show ferroelectric behaviour while when doped by La or Sn both these systems show relaxor behaviour [13,14].

Raman spectroscopy is a powerful tool to study local disorder and to detect PNRs. The appearance of polar modes reveals the existence of PNRs in Raman spectroscopy measurements. Although a lot of work is reported about the detection of the PNRs by x-ray diffraction, neutron diffraction, polarized Raman spectroscopy and IR spectroscopy [3,4,15,16,17,18], there are very few reports on the effect of growth and dynamics of the PNRs on the polar modes [19,20]. The polar modes are a direct signature of the polarity and hence it should provide direct information about the growth, dynamics and quasistatic freezing of the PNRs denoted by the characteristic temperatures of the relaxor system as mentioned above.

In order to investigate the behaviour of polar modes in relaxors, we chose Pr doped SrTiO<sub>3</sub> system. SrTiO<sub>3</sub> (STO) is a known quantum paraelectric which shows tetragonal transition through antiferro distortion (AFD) below 105 K. This compound, thus shows AFD modes below 105 K in Raman spectroscopy but the spectra remains devoid of polar modes. When doped with Pr which has small ionic radii than the Sr ions, the system shows ferroelectricity at room temperature [21]. This compound showed centrosymmetric cubic structure for low  $x$  concentration ( $x \leq 0.075$ ) and tetragonal structure at high doping values. The ferroelectricity in this compound was highly debated because of the presence of the global centrosymmetric structure. The issue is settled when Garg et al [22] conclusively showed from their high resolution x-ray and neutron diffraction measurements that the system is globally

centrosymmetric but retains non-centrosymmetric distortions at local level and the behaviour is best described in the frame work of relaxor ferroelectrics. Checchia *et al* [23] carried out detailed x-ray diffraction studies on this series of compounds and observed room-temperature tetragonal structure ( $I4/mcm$ ) for compositions with  $x \geq 0.1$ , whereas cubic structure for compositions with  $x \leq 0.075$  at room temperature. The existence of PNRs at room temperature was confirmed by the observation of polar modes in the Raman spectroscopy study in all the doped compositions at room temperature. It was also shown that the local tilting angle of the oxygen octahedra surrounding the Ti ions is active in all the compositions independent of their long range symmetry. Their experimental results also supported coexisting AFD and FE instabilities predicted by Aschauer and Spaldin [24] in their theoretical studies.

In this report we carried out detailed Raman spectroscopy studies from 80 K to 1018 K on polycrystalline  $Sr_{1-x}Pr_xTiO_3$  ( $x=0.01, 0.025, 0.05, \text{ and } 0.075$ ) samples. In all the samples The  $TO_2$  Polar mode showed anomalous behaviour upto  $T^*$  and the polar mode showed waning with increasing temperature but could be observed up to 1018 K in all the samples.

### Experimental:

The  $Sr_{1-x}Pr_xTiO_3$  ceramic compounds ( $x= 0.010, 0.025, 0.050, 0.075$ ) were prepared using conventional solid state reaction route. Stoichiometric ratios of the high purity (99.99%)  $SrCO_3$ ,  $Pr_6O_{11}$ ,  $TiO_2$  (Alpha Aesar) precursors were mixed using a mortar and pestle for 6-8 hours with acetone as an intermediate media. The mixed samples were calcined at  $1150^\circ C$  for 10 hours. After the cooling, the calcined sample was grinded again for 6-8 hours and pressed uniaxial in 10 mm pallets. These pallets were sintered at  $1420^\circ C$  for 12 hours. The process was repeated until single phase compound was obtained. The obtained samples were characterized by High resolution X-ray diffraction and Raman spectroscopic measurements. High resolution X-ray diffraction measurements were performed using  $Cu K\alpha$  radiation Lab source (Bruker) with step size of  $0.02^\circ$ . The Raman measurements were carried out using Horiba JY make HR-800 single spectrometer with an 1800 g/mm grating and a CCD detector. We used a He-Ne excitation source (633 nm) laser beam focused into  $\sim 1\mu m$  diameter spot with backscattering geometry where the incident light is linearly polarized and spectral detection is unpolarized. An Olympus microscope was used to view the images of the surface of the sample and a LMplanFI 50X lens during our measurements. The overall spectral resolution of the system is  $\sim 1\text{ cm}^{-1}$ . The temperature dependent Raman

measurements were performed by mounting the pressed pellet of doped  $SrTiO_3$  in, Linkam, U.K. make THMS600 stage for the low temperature measurements (80-300 K) and a Linkam, U.K. make TS1000 stage for the high temperature measurements (300-1018 K), having a temperature stability of  $\pm 0.1\text{ K}$ . Raman spectrum was collected for 40 sec exposures for all the samples in complete temperature range of 80-1018 K.

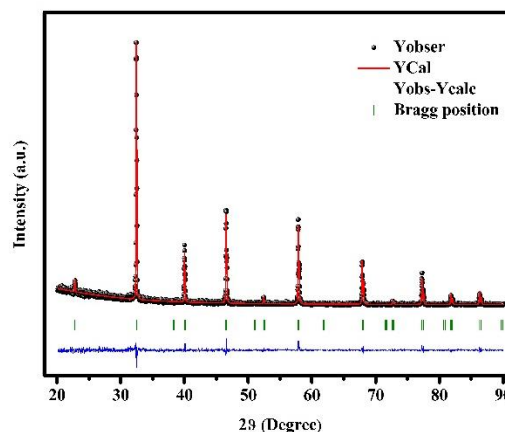


**Figure1:** The experimental x-ray diffraction pattern measured in  $\theta$ - $2\theta$  geometry (dots) along with fitted curve obtained using Rietveld refinement (line) and the difference plot at the bottom of the curve. The vertical ticks in the figure represents the position of the Bragg reflections.

### Results:

The x-ray diffraction measurements were carried out in order to assess the long range symmetry of the samples. Figure 1 shows the representative x-ray diffraction pattern for  $x=0.075$  composition. The dots represent experimental data while the line denotes the fitted curve generated by refinement of the x-ray diffraction pattern using FullProf software [25]. The patterns could be well fitted by using cubic symmetry with  $Pm\bar{3}m$  space group for compositions  $x < 0.075$  with satisfactory goodness of fit parameters. Garg *et al* [22] reported tetragonal symmetry for  $x \geq 0.05$  compositions from neutron and Raman scattering measurements while Checchia *et al* [2323] reported cubic symmetry up to  $x=0.075$  from their x-ray diffraction measurements. The  $x=0.075$  composition was therefore attempted to be fitted with cubic as well as tetragonal space group ( $I4/mcm$ ). The goodness of fit parameters as well difference plots were seen to be comparable for fitting considering tetragonal symmetry and cubic symmetry. Therefore, from our laboratory x-ray diffraction pattern we could not conclusively establish the symmetry of this sample.

In order to access the local symmetry of these samples, room temperature Raman characterization

was carried out and is presented in Figure 2. For low doped compositions i.e.  $x=0.01$  and  $0.025$  five Raman modes are observed at  $117, 127, 175, 540, 795 \text{ cm}^{-1}$ ; the position of these modes matched with previous reports

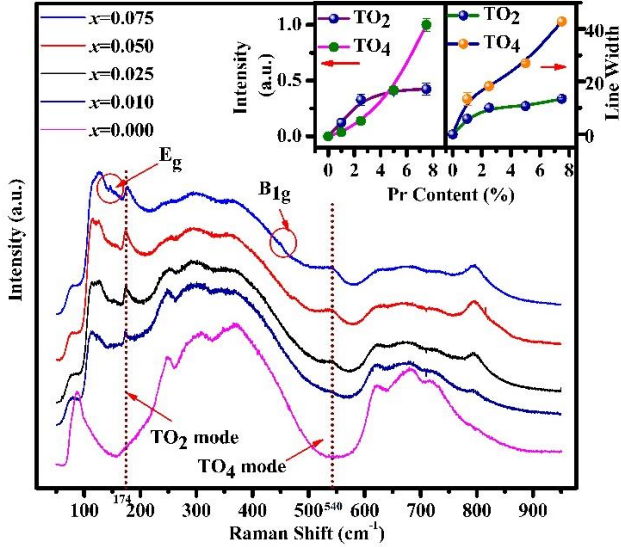


**Figure 2:** The Raman spectra of  $\text{Sr}_{1-x}\text{Pr}_x\text{TiO}_3$  ( $x=0.0, 0.010, 0.025, 0.050, 0.075$ ) collected at room temperature. The spectra are shifted vertically for clarity. The Inset shows the normalized intensity (left) and FWHM (right) of the polar modes as a function of  $x$ .

[23, 26, 27]. As such for  $\text{SrTiO}_3$ ; first order Raman scattering is forbidden in the cubic symmetry shown by this compound at room temperature, but the presence of guest or impurity atoms (Pr in present case) relaxes the selection rules and gives rise to first order scattering. Apart from these modes a feeble mode is observed at  $475 \text{ cm}^{-1}$  which is assigned as  $\text{LO}_3$  mode in the literature. For  $x=0.075$  composition, two additional modes are observed at  $145 \text{ cm}^{-1}$  and  $445 \text{ cm}^{-1}$ . The position of these modes matches with  $E_g$  and  $B_{1g}$  modes observed in pure  $\text{SrTiO}_3$  below  $105 \text{ K}$ . These modes arise out of AFD in tetragonal symmetry due to bending of octahedron as  $a^0a^0c^-$  [24] following Glazer scheme of notations. From previous results [23, 28] we have assigned the remaining Raman modes falling at  $175, 540, 795 \text{ cm}^{-1}$  as  $\text{TO}_2, \text{TO}_4$  and  $\text{LO}_4$  modes, respectively. The  $\text{TO}_2$  mode corresponds to polar last mode representing motion of Sr/Pr with respect to  $\text{TiO}_6$  octahedron while  $\text{TO}_4$  mode corresponds to polar axe mode arising due to bending of the octahedron [27]. Presence of the  $\text{TO}_2$  and  $\text{TO}_4$  modes in the Raman spectra has been

considered as an evidence of the presence of the polar instability [29, 30] in the system. The distortion of unit cell from cubic to tetragonal unit cell at lower temperature originate from antiferrodistortive (AFD) transition which makes the  $E_g$  and  $B_{1g}$  modes Raman active. Absence of these modes at room temperature in low doped samples confirms cubic symmetry. However, its observation in

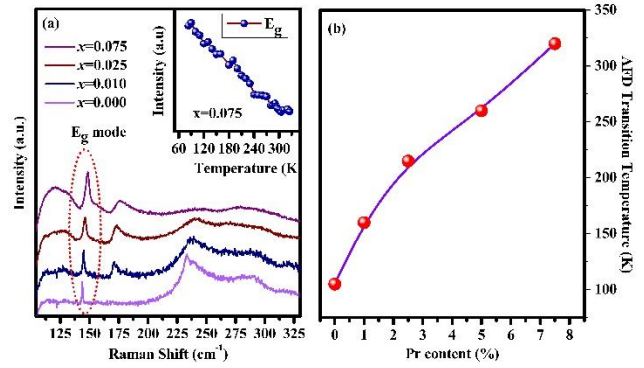


**Figure 3:** (a) The Raman spectra of  $\text{Sr}_{1-x}\text{Pr}_x\text{TiO}_3$  ( $x=0.0, 0.010, 0.025, 0.075$ ) collected at  $83 \text{ K}$ . The inset shows the variation of  $E_g$  mode intensity as a function of temperature for  $x=0.075$ . (b) The AFD transition temperature as a function of  $x$ .

$x=0.075$  at room temperature, conforms tetragonal symmetry in  $x=0.075$  at room temperature.  $E_g$  and  $B_{1g}$  modes represents  $\text{TiO}_6$  octahedral tilt around  $c$ -axes which occurs from condensation of triply degenerate  $R_{25}$  phonon [23, 28]. The spectra were fitted using multiple Lorentz functions and the intensity and line width of the polar modes as a function of composition is presented in the inset of the Figure 2. It is observed that with increase in  $x$ , the intensity of the  $\text{TO}_2$  and  $\text{TO}_4$  polar modes increases. The line width of the  $\text{TO}_4$  mode also showed an increase with increasing composition. Also the position of the  $\text{TO}_2$  mode shows a shift towards higher wavenumber as the doping is increased though the variation is small. The increase in wavenumber with increasing  $x$  can be considered as due to incorporation of heavier Pr atoms instead of Sr atoms, resulting in hardening of force constant of the lattice vibration [31]. The increased line width with increasing  $x$ , suggests decrease in phonon life time due to incorporation of larger site distortion in the system. Another important observation from room temperature results is intense TO mode intensity. Such strong intensity of the TO modes were not reported in other compounds. This can be due to preserving nature of Pr ions towards ferroic character [32] which not only

causes first order scattering due to local symmetry lowering but also these distortions are strongly coupled to optical modes and hence enhances local scattering [33]. From XRD and Raman characterization, we thus conclude that globally all the studied compositions conform cubic symmetry except for  $x=0.075$ . This composition shows sign of tetragonal symmetry at room temperature. However, the local symmetry of all the samples is lower than the cubic symmetry resulting in first order Raman scattering. Interestingly, the second order Raman scattering modes of the system remain unaffected due to doping. LO<sub>4</sub> modes which arises from Pr introduction in STO matrix becomes broad and intense.

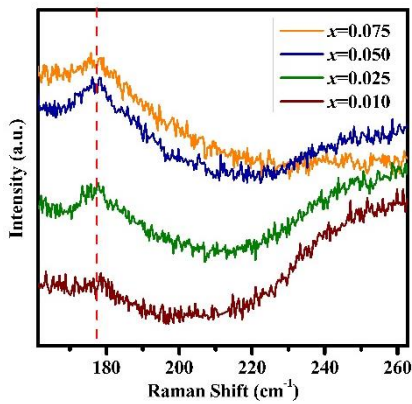


**Figure 4:** The Raman spectra of  $\text{Sr}_{1-x}\text{Pr}_x\text{TiO}_3$  ( $x=0.010, 0.025, 0.050, 0.075$ ) collected at 1018 K showing  $\text{TO}_2$  mode (vertical dashed line).

Figure 3 (a) shows the normalized Raman spectra of all the compositions at 83 K. The spectra are shifted vertically for clarity. For better comparison, the Raman spectra of the  $\text{SrTiO}_3$  single crystal is also included. The single crystal used in the present study is a commercially brought substrate (MTI Corporation, USA). It is noted that the  $\text{TO}_2$  mode ( $\sim 174 \text{ cm}^{-1}$ ) is observed in all the compositions except for undoped  $\text{SrTiO}_3$ . This mode showed hardening, increase in intensity and decrease in asymmetry with increasing  $x$ . The line width also showed significant increase with increasing  $x$ . Similarly, the  $E_g$  mode which is a signature of tetragonal symmetry is observed in all the samples and its intensity, line width and position showed an increase with increasing  $x$ . The increase in line width of the  $E_g$  mode reflects the site disorder induced due to Pr doping. It is worth noting that the intensity of polar mode ( $\text{TO}_2$ ) as well as AFD mode ( $E_g$ ) show an increase with increasing  $x$ . This clearly suggests the one to one correspondence between

polarities of the sample and the tetragonal distortion. This is against the general paradigm that the polar distortion and AFD competes and cancels [34]. The behaviour of  $E_g$  mode intensity as a function of temperature for  $x=0.075$  composition is plotted in the inset of Figure 3 (a). It showed a normal behaviour that is nearly linear decrease in intensity with increase in temperature and it gets completely suppressed above 320 K. It is noted from this figure that the AFD distortions increases with increasing  $x$ . From the  $E_g$  mode, the cubic to AFD transition was also deduced as a function of temperature and is plotted in figure 3 (b). The transition temperature increases linearly with increase in  $x$ . From this it can be concluded that the AFD and Polar distortions both increases with increasing  $x$ .

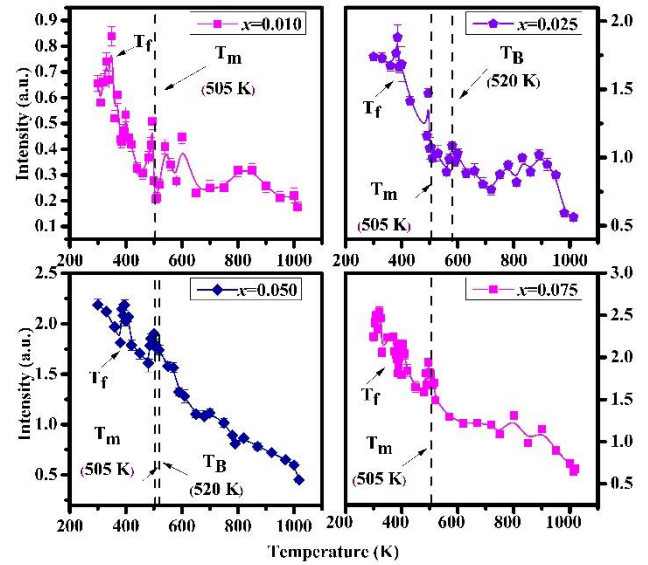


**Figure 5:** Intensity of the  $\text{TO}_2$  mode as a function of temperature for different compositions. The vertical dashed lines denote  $T_m$  and  $T_B$  for the respective compositions.

In order to observe the changes in the Raman spectra across the  $T_m$ ,  $T^*$  and  $T_B$ , temperature dependent Raman spectroscopy studies on all the samples were carried out from room temperature to 1018 K. The spectra showed expected changes with increasing temperature i.e. the Raman modes showed suppression and increased line width with increasing temperature. Most of the modes diminished at higher temperatures except  $\text{TO}_2$  mode. The spectra collected at 1018 K is presented in figure 4. At such an elevated temperature also,  $\text{TO}_2$  mode is observable for all the doped compositions. This suggests that the weak local polar distortions remain present in all the doped compositions up to very high temperatures.

The temperature dependent spectra is fitted using multiple Lorentz functions and the intensity, position and line width of the TO<sub>2</sub> and TO<sub>4</sub> modes were obtained as a function of temperature. The temperature dependence of the intensity of the TO<sub>2</sub> mode is plotted in figure 5 for all the four samples. It is noted that the intensity showed modulations around the characteristic temperatures: just below  $T_c$  i.e. between 350-400 K (marked by an arrow) representing freezing of PNRs and in the vicinity of the dielectric anomaly temperature. Similarly, the intensity of the TO<sub>4</sub> mode (not shown here) also showed some weak signatures of modulation around the characteristic temperatures, however, the mode is found to be very broad and weak

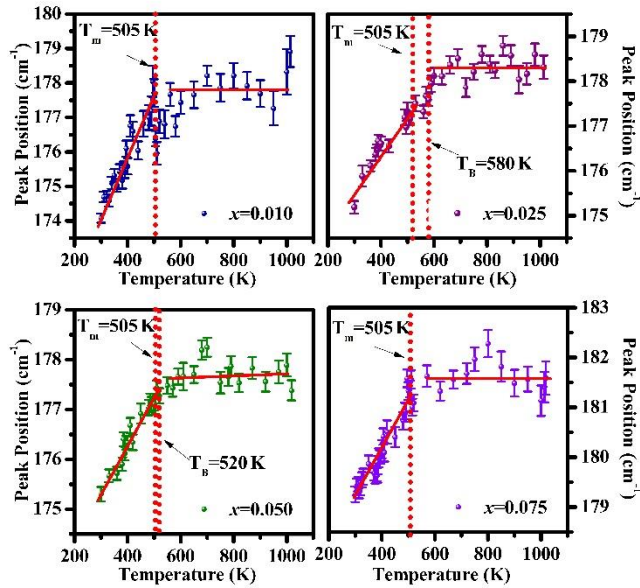


**Figure 6:** The Raman shift of TO<sub>2</sub> mode as function of temperature for various compositions. The lines over the data are guide to the eye while the vertical dashed lines denote the characteristic temperatures,  $T_m$  and  $T_B$ .

in most of the compositions which resulted in large error bars in the intensity at high temperatures. The mode position of the TO<sub>2</sub> mode as a function of temperature is plotted in figure 6, the data is represented by dots while the line is a guide to the eye. It showed anomalous behaviour of the mode wavenumber up to a temperature which is in between  $T_m$  and  $T_B$ , the wavenumber showed an increase with increasing temperature. After this the temperature variation of the mode frequency showed a change in slope and then it shows a constant variation at elevated temperatures, upto 1018 K. The mode wavenumber of the TO<sub>4</sub> mode is also plotted against temperature which unlike TO<sub>2</sub> mode, showed a monotonous normal behaviour (Figure 7). The mode frequency as a function of temperature of the TO<sub>4</sub> mode was fitted using anharmonic function for three phonon processes following Balakansi et al [35] and is shown by a line.

## Discussions:

The properties of relaxor ferroelectrics are known to be governed by the nucleation and growth of the PNRs. The static and dynamic structure of these PNRs shapes the relaxor mechanism. The short range ferroelectric order due to breaking of local centro-symmetry is responsible for the growth of PNRs. The breaking of centro-symmetry locally is previously reported to be due to either strain or doping induced disorder. In Pr doped SrTiO<sub>3</sub> the A-site doping induced disorder is responsible for the breaking of cubic symmetry locally. The fluctuation in chemical compositions at A-site results in regions that encapsulates highly distorted

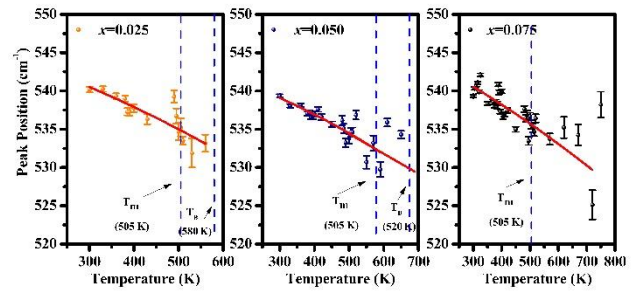


**Figure 7:** The Raman shift of TO<sub>4</sub> mode as a function of temperature for various compositions. The line represents the fitted curve generated using anharmonic model.

octahedra compared to other regions where the octahedra is more symmetric. Our Raman scattering studies clearly showed enhanced signatures of the presence of AFD in doped samples when compared to undoped samples. The AFD transition temperature is shown to increase with increasing doping concentration of Pr. The intensity of the TO<sub>2</sub> mode which is a signature of polarity generated due to off-centering of A-site ions showed correlation with the AFD mode intensity. Thus, our studies once again supports the observations presented in reference [23, 36] that the AFD and ferroelectric instabilities cooperate at local length scale. The TO<sub>4</sub> mode intensity was found to be subdued which is expected as this mode arises due to oxygen octahedral rotation inducing off-centering of the Ti ions. Thus, present study once again provides an evidence that the PNRs are generated due to A-site off-centering.

Another interesting observation is the anomalous behaviour of TO<sub>2</sub> mode as a function of temperature. This mode shows hardening when temperature is raised. It showed a change of slope just below  $T_m$ , and a further change in behaviour after  $T_B$ . The TO<sub>2</sub> mode softening observed just below  $T_m$  indicates its relation

with slowing down of the dynamics of the PNRs or freezing of PNRs. In a perfect ferroelectric material, the dielectric maxima represent change in order parameter (global) related to paraelectric to ferroelectric phase transition. Similarly, the dielectric maxima observed in relaxor ferroelectrics can be considered as a signature of change in local order parameter related to local ferroelectric order in the matrix of paraelectric phase. The ferroelectric order is always related with dipole-dipole interaction. The TO<sub>2</sub> phonon mode which is arising due to local fluctuations in centro-symmetry is likely to be strongly coupled with the dipole-dipole interaction responsible for local ferroelectric order. The anomalous softening of the TO<sub>2</sub> mode below T\* reveals the strong coupling between local dipolar order and polar phonon. The present study clearly shows the modulation in the TO<sub>2</sub> phonon mode frequency due to setting in of dipolar order or in other words the renormalization of the TO<sub>2</sub> phonon mode due to local ferroelectric order.

## References:

- <sup>1</sup> L. E. Cross, *Ferroelectrics*, **76**, 241–67, (1987).
- <sup>2</sup> R. Pirc and R. Blinc, *Phys. Rev. B* **60**, 13470, (1999).
- <sup>3</sup> N Waesermann et al *J. Phys.: Condens. Matter* **25**, 155902, 2013.
- <sup>4</sup> Aneta Slodczyk, Philippe Daniel, and Antoni Kania, *Phys. Rev. B* **77**, 184114, (2008).
- <sup>5</sup> B. Mihailova et al, *Phys. Rev. B* **77**, 174106, (2008).
- <sup>6</sup> I. W. Chen, P. Li, and Y. Wang, *J. Phys. Chem. Solids* **57**, 1525, (1996).
- <sup>7</sup> I. W. Chen, *J. Phys. Chem. Solids* **61**, 197, (2000).
- <sup>8</sup> K. Fujishiro, T. Iwase, Y. Uesu, Y. Yamada, B. Dkhil, J.-M. Kiat, S. Mori, and N. Yamamoto, *J. Phys. Soc. Jpn.* **69**, 2331, (2000).
- <sup>9</sup> E. Prouzet, E. Husson, N. de Mathan, and A. Morell, *J. Phys.: Condens. Matter* **5**, 4889, (1993).
- <sup>10</sup> V. A. Shuvaeva, I. Pirog, Y. Azuma, K. Yagi, K. Sakaue, H. Terauchi, I. P. Raevskii, K. Zhuchkov, and M. Yu Antipin, *J. Phys.: Condens. Matter* **15**, 2413, (2003).
- <sup>11</sup> Badari Narayana Rao, Ranjan Datta, S. Selva Chandrashekar, Dileep K. Mishra, Vasant Sathe, Anatoliy Senyshyn, and Rajeev Ranjan, *Phys. Rev. B* **88**, 224103, (2013).
- <sup>12</sup> O. Hanske-Petitpierre, Y. Yacoby, J. Mustre de Leon, E. A. Stern, and J. J. Rehr, *Phys. Rev. B* **44**, 6700, (1991).
- <sup>13</sup> Xunhu Dai, Z. Xu, and Dwight Viehland, *J. Appl. Phys.* **79**, 1021–1026, (1996).
- <sup>14</sup> Shi, T., Xie, L., Gu, L. & Zhu, *J. Sci. Rep.* **5**, 8606; DOI:10.1038/srep08606, (2015).
- <sup>15</sup> Guangyong Xu, P. M. Gehring, and G. Shirane *Phys. Rev. B* **74**, 104110, (2006).
- <sup>16</sup> Badari Narayana Rao, Dipak Kumar Khatua, Rohini Garg, Anatoliy Senyshyn, and Rajeev Ranjan *Phys. Rev. B* **91**, 214116, (2015).
- <sup>17</sup> B.E. Vugmeister, P. DiAntonio, and J. Toulouse, *Phys. Rev. Lett.* **75**, 1646, (1995)
- <sup>18</sup> C. Stock, Guangyong Xu, P. M. Gehring, H. Luo, X. Zhao, H. Cao, J. F. Li, D. Viehland, and G. Shirane *Phys. Rev. B* **76**, 064122, (2007).
- <sup>19</sup> D. A. Tenne, A. Soukiassian, X. X. Xi, H. Choosuan, R. Guo, and A. S. Bhalla; *Phys. Rev. B* **70**, 174302, (2004).
- <sup>20</sup> B Hehlen et al *J. Phys.: Condens. Matter* **26**, 015401, (2014)
- <sup>21</sup> A. Durán, E. Martínez, J. A. Díaz, and J. M. Siqueiros, *J. Appl. Phys.* **97**, 104109, (2005).
- <sup>22</sup> R. Garg, A. Senyshyn, H. Boysen, R. Ranjan, *Phys. Rev. B* **79**, 144122, (2009).
- <sup>23</sup> Stefano Checchia, Mattia Allietta, Mauro Coduri, Michela Brunelli, and Marco Scavini *Phys. Rev. B* **94**, 104201, (2016).
- <sup>24</sup> Ulrich Aschauer and Nicola A Spaldin *J. Phys.: Condens. Matter* **26**, 122203, (2014)
- <sup>25</sup> Carvajal J R *Physica B* **190**, 55-69, (1993)
- <sup>26</sup> Rajeev Ranjan, Rohini Garg, Rudi Hackl, Anatoliy Senyshyn, Elmar Schmidbauer, Dmytro Trots, and Hans Boysen, *Phys. Rev. B* **78**, 092102 (2008)
- <sup>27</sup> V. Goian, S. Kamba, J. Hlinka, P. Vanek, A.A. Belik, T. Kolodiaznyy, and J. Petzelt, *Eur. Phys. J. B* **71**, 429–433 (2009)
- <sup>28</sup> Rajeev Ranjan, Rudi Hackl, Amreesh Chandra, Elmar Schmidbauer, Dmytro Trots, and Hans Boysen *Phys. Rev. B* **76**, 224109 (2007).
- <sup>29</sup> U. Bianchi, W. Kleemann, and J. G. Bednorz, *J. Phys.: Condens. Matter* **6**, 1229 (1994)
- <sup>30</sup> P. DiAntonio, B. E. Vugmeister, J. Toulouse, and L. A. Boatner, *Phys. Rev. B* **47**, 5629 (1993)
- <sup>31</sup> J. Frantti and V. Lantto *Phys. Rev. B* **54**, 12139 (1996)
- <sup>32</sup> A. K. Kalyani, R. Garg and R. Ranjan, *Appl. Phys. Lett.*, **95**, 222904, (2009).
- <sup>33</sup> Seiji Kojima et al *J. Phys.: Conf. Ser.* **428**, 012027 (2013).

---

<sup>34</sup> W. Zhong and D. Vanderbilt, *Phys. Rev. Lett.* **74** 2587 (1995).

<sup>35</sup> Balakansi et al *Phys. Rev. B*, **28**, 1928, (1983).

<sup>36</sup> Shekhar Tyagi, Gaurav Sharma, Vasant G Sathe, *J. Phys.: Condens. Matter* **30**, 105401 (2018).